Inducing Synergy in Bimetallic RhNi Catalysts for CO_2 Methanation by Galvanic Replacement

Yuan Wang,[a,b,c] Hamidreza Arandiyan,[d,*] Stuart A. Bartlett,[d] Annette Trunschke,[c,*] Hongyu Sun,[e] Jason Scott,[a,*] Adam F. Lee,[f,*] Karen Wilson,[f] Thomas Maschmeyer,[d] Robert Schlögl,[c] and Rose Amal[a]

Dr. Yuan Wang, A/Prof. Jason Scott, and Prof. Rose Amal

[a]*Particles and Catalysis Research Group, School of Chemical Engineering, The University of New South Wales, Sydney 2052, Australia*

Dr. Yuan Wang

[b]*School of Chemistry, Faculty of Science, The University of New South Wales, Sydney, New South Wales, Australia*

Dr. Annette Trunschke, Dr. Yuan Wang and Prof. Robert Schlögl

[c]*Inorganic Chemistry Department, Fritz-Haber-Institut der Max-Planck-Gesellschaft, Faradayweg 4-6, 14195 Berlin, Germany*

Dr. Hamidreza Arandiyan, Dr. Stuart A. Bartlett, and Prof. Thomas Maschmeyer

[d]*Laboratory of Advanced Catalysis for Sustainability, School of Chemistry, The University of Sydney, Sydney 2006, Australia*

Dr. Hongyu Sun

[e]*Department of Micro- and Nanotechnology, Technical University of Denmark, Kongens Lyngby 2800, Denmark*

Prof. Karen Wilson, and Prof. Adam F. Lee

[f]*School of Science, Royal Melbourne Institute of Technology University, Melbourne, VIC 3000, Australia*

** Corresponding authors E-mail address: hamid.arandiyan@sydney.edu.au (H.A.), adam.lee2@rmit.edu.au (A.F.L.) jason.scott@unsw.edu.au (J.S.), trunschke@fhi-berlin.mpg.de (A.T.)*

S1. Catalyst characterisation

S1.1. X-ray diffraction (XRD)

XRD analyses were performed on a PANalytical Empyrean II diffractometer with Cu Kα radiation (λ = 0.15406 nm) at 45 kV and 40 mA to identify the crystal phases and to analyse lattice parameters. Scattering intensity was recorded in the range of 30° < 2θ < 90° for all of the samples with a 2θ step of 0.03° and a count time of 2 s per step. Diffraction patterns were indexed to JCPDS (Joint Committee on Powder Diffraction Standards) files.

S1.2. Field-emission high-resolution transmission electron microscopy (FE-HRTEM) and high-angle annular dark-field - scanning transmission electron microscopy energy-dispersive X-ray spectroscopy (HAADF-STEM-EDS)

FE-HRTEM images, as well as the selected-area electron diffraction (SAED) patterns, were obtained on a Philips CM200 apparatus. To determine the detailed surface structure, HAADF-STEM-EDS images were taken on a JEOL JEM-ARM200F STEM.

S1.3. BET surface area and N_2 adsorption-desorption isotherm

The surface areas and pore size distributions of the samples were obtained using the Brunauer-Emmett-Teller (BET) and Barrett-Joyner-Halenda (BJH) methods, respectively. The N_2 adsorption-desorption isotherms, surface areas, and pore parameters of the samples were determined via N_2 adsorption at –196 °C on a Micrometric Tristar 3030 adsorption analyser. Before the measurement, the samples were degassed at 150 °C for 3 h.

S1.4. H_2 temperature-programmed reduction (H_2-TPR)

H_2-TPR experiments were performed on a Micromeritics Autochem II apparatus equipped with a TCD detector. The experiments were conducted with approximately 50 mg of sample. The samples were initially flushed with an argon flow of 40 mL/min as the temperature was increased to 150 °C at a ramp rate of 10 °C/min. The samples were kept at this temperature for 30 min to remove moisture after which they were cooled to 50 °C. Then, the reducing gas (10 % H_2 in Ar) was introduced at a flow rate of 40 mL/min and the sample was heated at a ramp rate of 10 °C/min to 900 °C. The variation in H_2 concentration of the effluent gas stream was monitored online by the TCD.

S1.5. X-ray photoelectron spectroscopy (XPS)

XPS was used to determine the Rh 3d binding energies (BEs) of surface species. The analyses were performed on a Thermo Scientific, UK (model ESCALAB250Xi) using Mg Kα ($h\nu$ = 1486.68 eV) as the excitation source with 150 W power (13 kV x 12 mA). Samples were reduced at 400 °C for 1 h prior to XPS analysis to mimic the activation protocol employed for CO_2 methanation; however, they were subsequently air-exposed for 3-5 days awaiting transfer to the spectrometer chamber. Sample were then outgassed (0.5 h) in the preparation chamber before being analysed in the analysis chamber. The BE values of Rh 3d were calibrated against the C 1s signal (BE = 284.6 eV for adventitious hydrocarbon) of carbon.

S1.6. Inductively coupled plasma mass spectroscopy (ICP-MS)

The actual loadings of Rh and Ni on the alumina support were measured by a Perkin Elmer OPTIMA 7300 ICP-MS. Samples were digested using aqua regia solution.

S1.7. X-ray absorption spectroscopy (XAS)

Rh K-edge X-ray absorption experiments were conducted at the Australian Synchrotron at the XAS beamline, collected in fluorescence mode using a 36 element Ge fluorescence detector. Samples were diluted with boron nitride and mounted using Kapton tape inside a He purged cell held at room temperature. Sample spectra were collected up to k =15 $Å^{-1}$ in parallel with a Rh foil reference. Data analysis was performed using the IFEFFIT software packages Athena and Artemis.

S2. Calculation of Rh dispersion:

The dispersion of a spherical, close-packed metal nanoparticle (NP) can be estimated from the particle size and atomic radius of constituent atoms according to the equation below:[1, 2]

$$Dispersion = \frac{N_S}{N_T} = \frac{R^3 - (R - \sqrt{3}r)^3}{R^3}$$

where R is the NP radius from HRTEM and r the atomic radius (lattice parameter: Rh = 3.80 nm; Ni = 3.52 nm). For $RhNi/Al_2O_3$ (GR), all the Rh appears to reside in a monolayer shell and hence the Rh dispersion is assumed to be 100 %. For Rh/Al_2O_3 the Rh dispersion is 70.3 %. For $RhNi/Al_2O_3$ (CR), the overall Rh:Ni atomic ratio is 0.91:1.79, and assuming the nanoparticles comprise a bulk substitutional alloy, Vegard's Law predicts a mean lattice parameter of 3.61 nm, and hence a total metal dispersion of 59 %; assuming a common surface and bulk Rh:Ni atomic ratio, the Rh dispersion is then 20 %. Note that CO and H_2 strongly chemisorb over Rh and Ni, and hence conventional chemisorption methods using these adsorbates would only provide the same information for the bimetallic catalysts as can be obtained by TEM analysis, i.e. the total metal dispersion.

Dispersions were used to calculate the turnover frequency (TOF) according to the following equation:

TOF = mols CO_2 converted.s^{-1}/ mols surface Rh

= mols CO_2 converted.s^{-1} / [(Dispersion × Rh loading (wt%) × catalyst mass)/ 100 × Molar mass Rh]

= mols CO_2 converted.s^{-1} / [(Dispersion × Rh loading × 0.05)/ 102.9]

S3. Experimental configuration and results

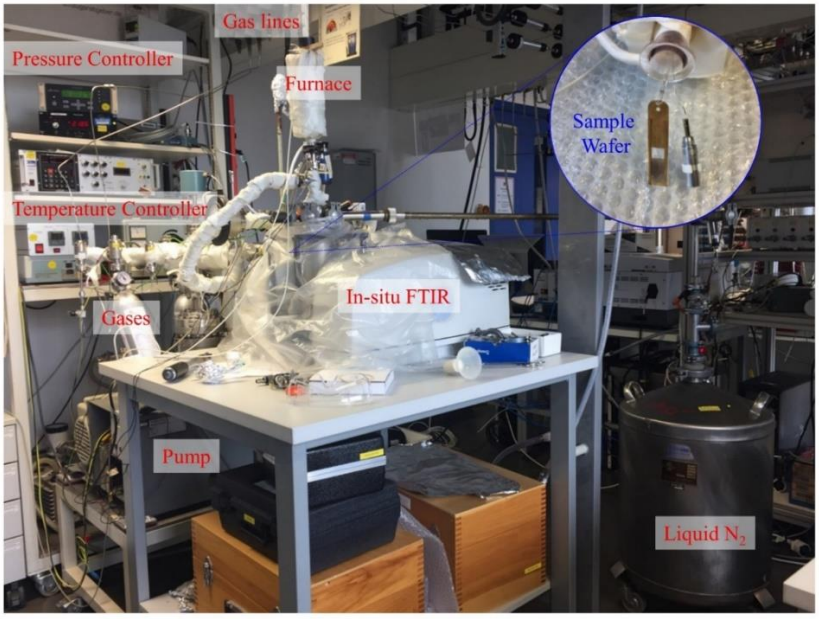

Fig. S1. Configuration of FTIR for low temperature CO adsorption.

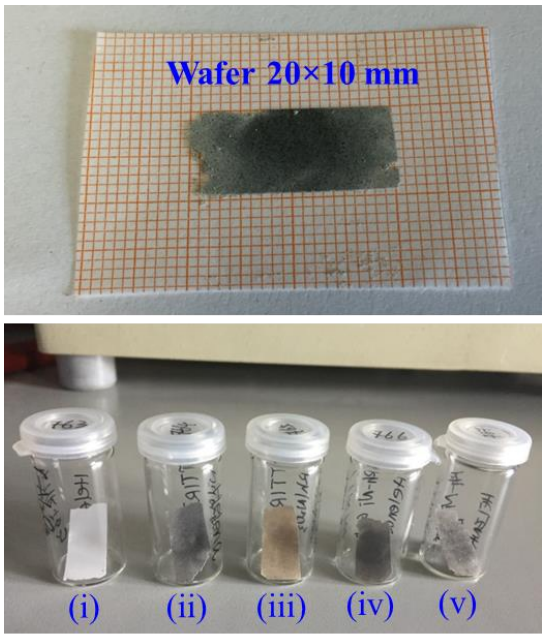

Fig. S2. Photos of sample wafers prepared for FTIR.

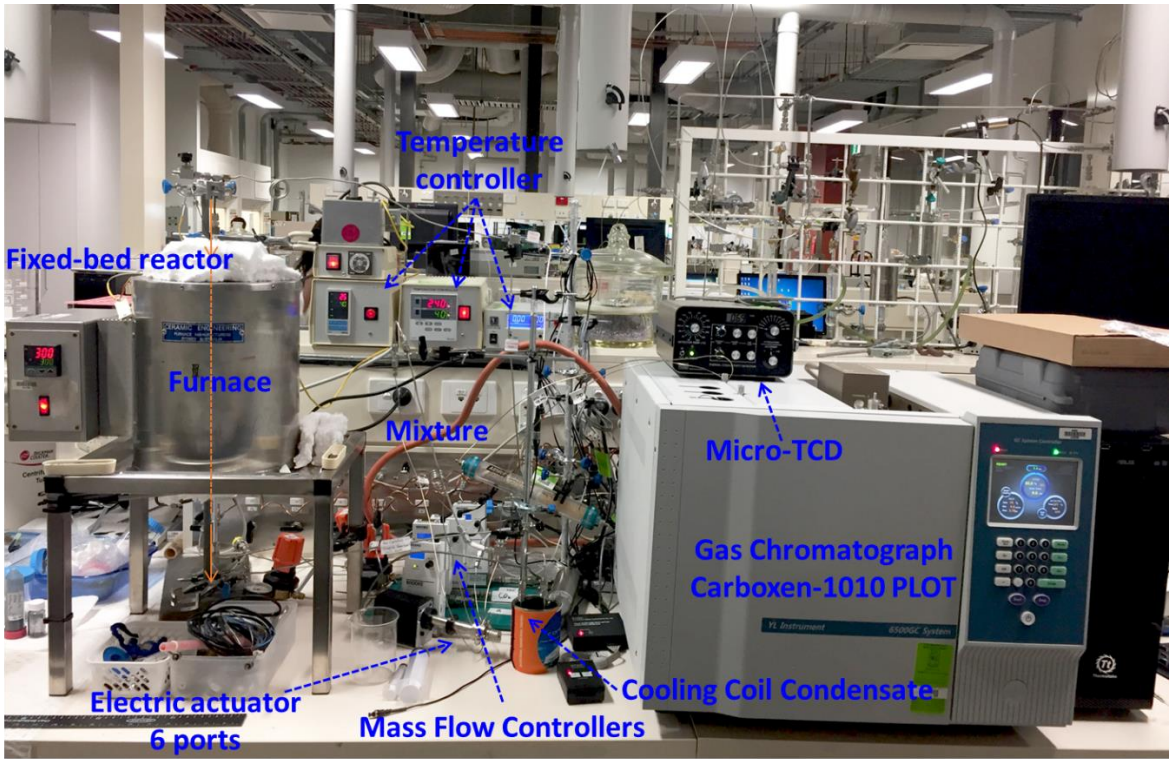

Fig. S3. Photograph of microreactor configuration for catalyst activity assessment.

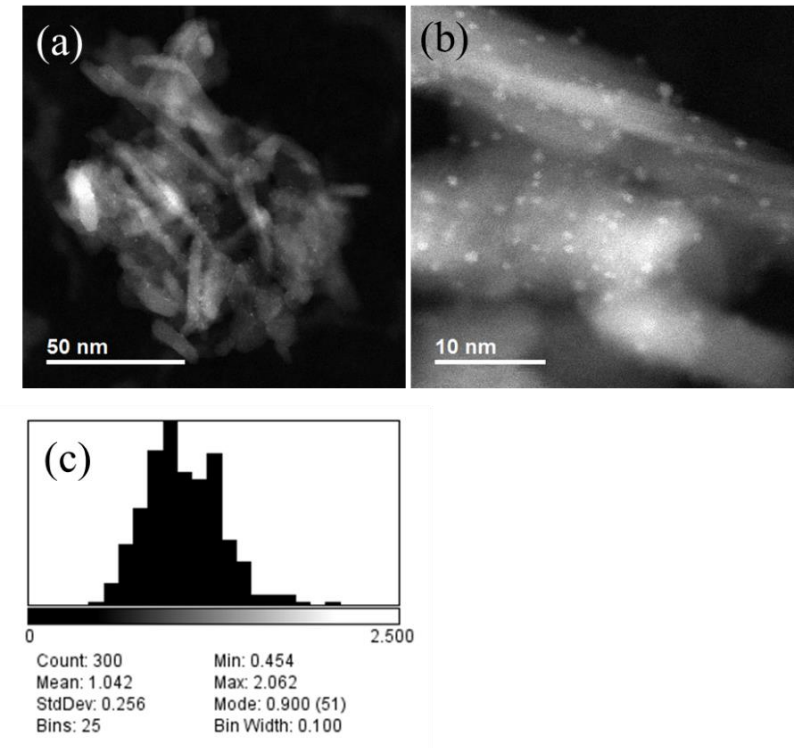

Fig. S4. (a-b) HAADF-STEM images and (c) nanoparticle size distribution for Rh/Al_2O_3.

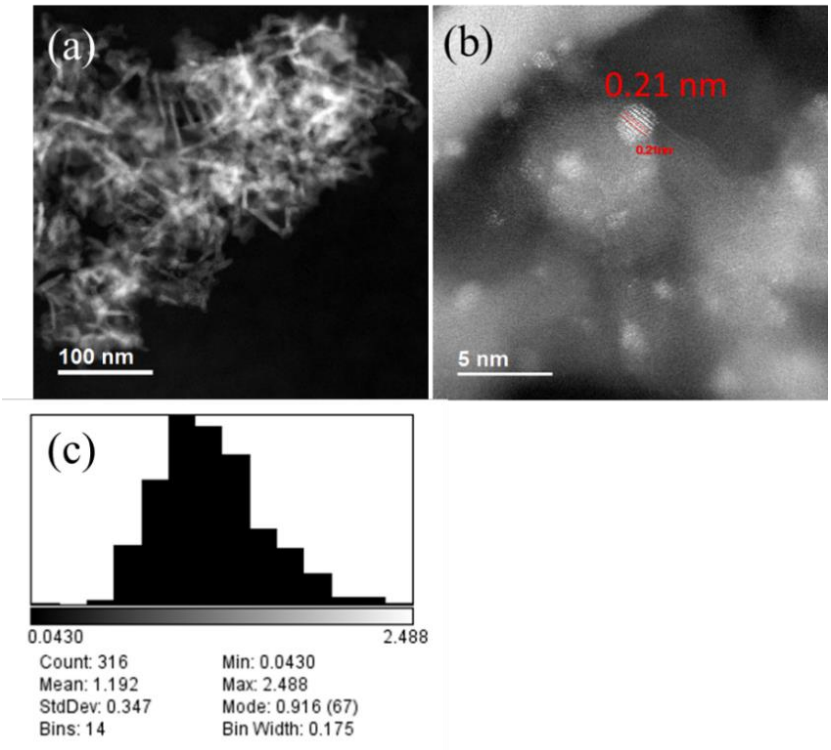

Fig. S5. (a-b) HAADF-STEM images and (c) nanoparticle size distribution for $RhNi/Al_2O_3$ (GR).

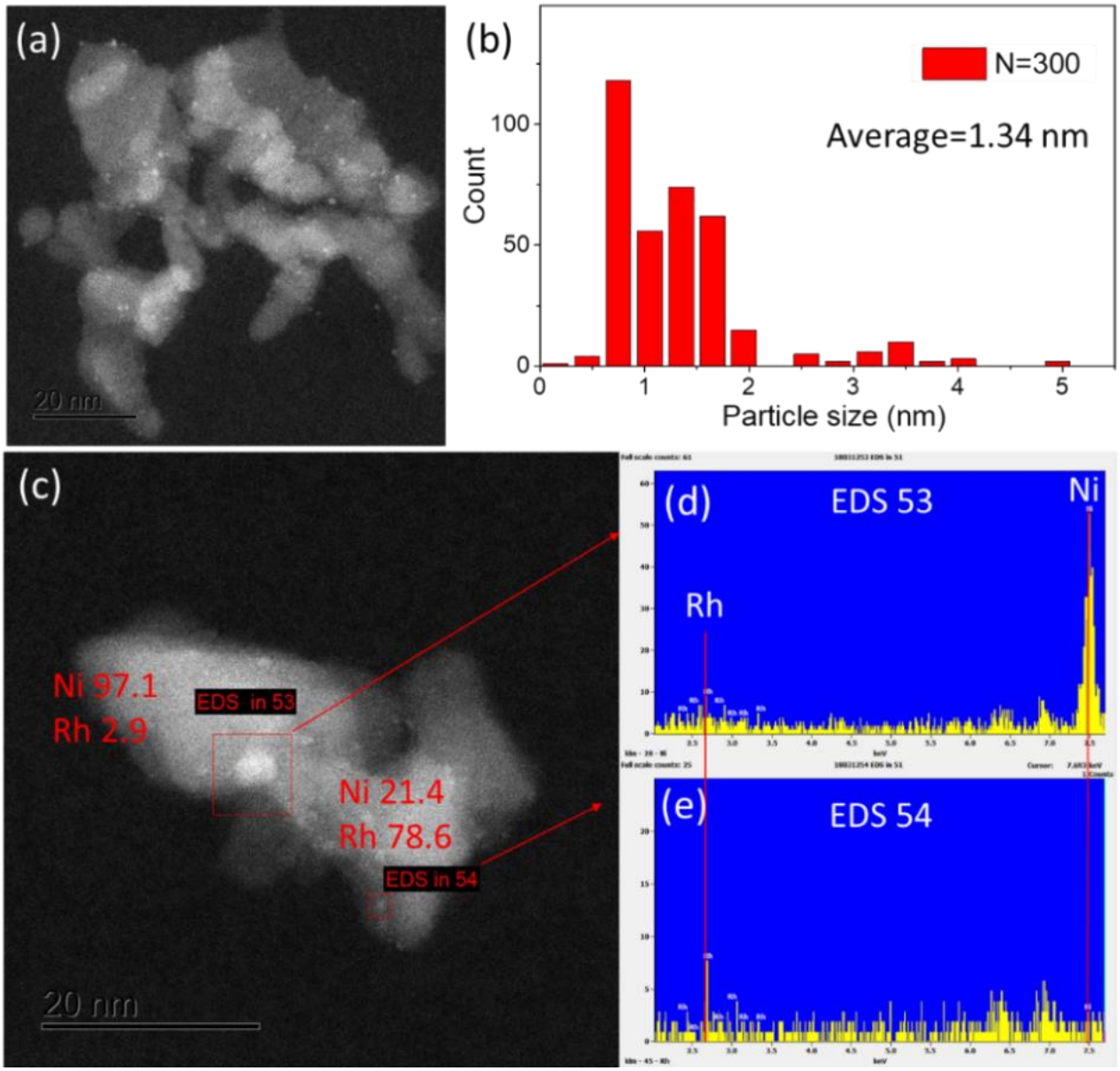

Fig. S6. (a) HAADF-STEM image, (b) nanoparticle size distribution, (c) HAADF-STEM image, and (d-e) EDS spectra extracted from red square in (c) for $RhNi/Al_2O_3$ (CR) sample.

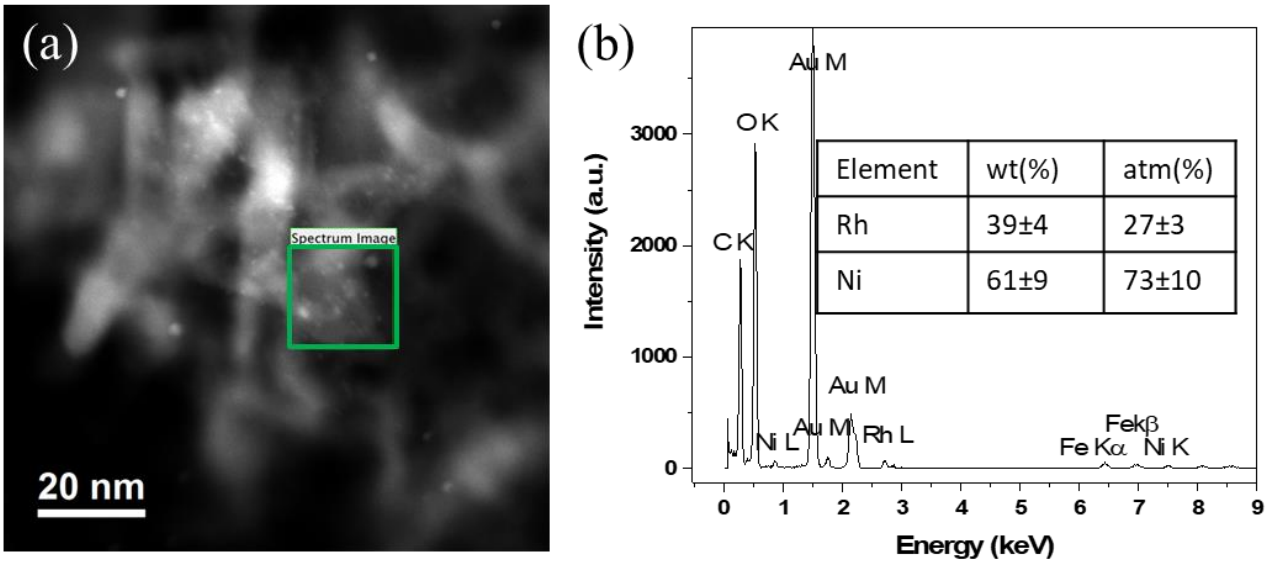

Fig. S7. (a) HAADF-STEM image and (b) EDS spectra and elemental (Rh, Ni) map for $RhNi/Al_2O_3$ (GR). Green square highlights sample region where EDS analysis was performed.

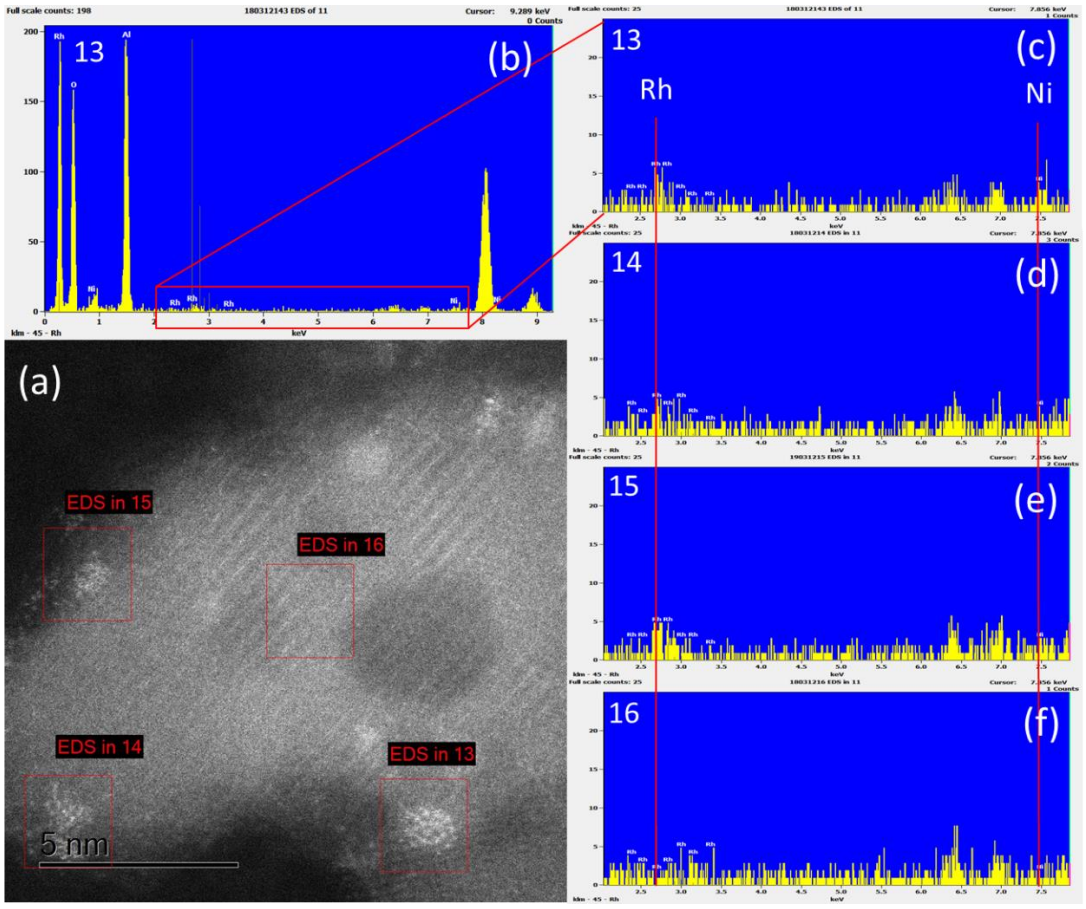

Fig. S8. (a) HAADF-STEM image and (b-f) EDS spectra of individual nanoparticles for $RhNi/Al_2O_3$ (GR). Numbers 13-16 in the EDS spectra refer to corresponding red squares in STEM image.

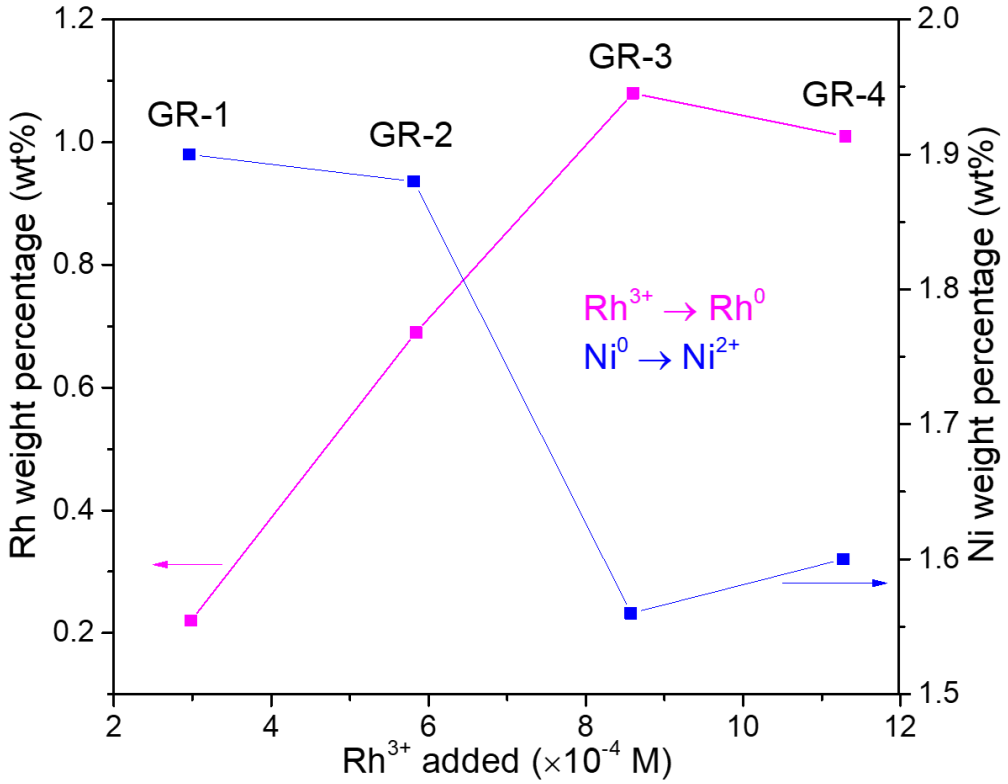

Fig. S9. Rh and Ni loadings versus concentration of Rh^{3+} precursor in the synthesis of RhNi GR catalysts.

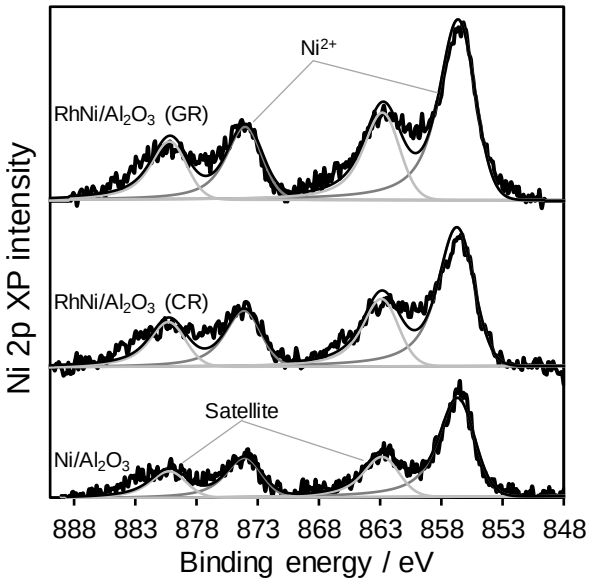

Fig. S10. Ni 2p XP spectra of Ni/Al_2O_3, $RhNi/Al_2O_3$ (GR) and $RhNi/Al_2O_3$ (CR). Spectra fitted with common lineshape, FWHM and binding energies.

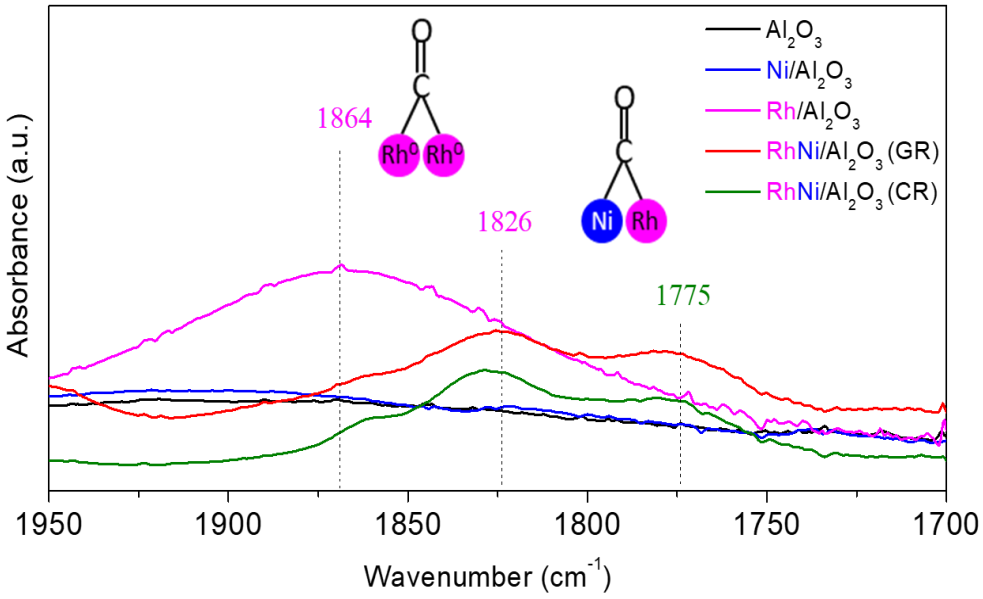

Fig. S11 FTIR spectra following CO saturation and purging with 40 mbar He at -196 °C.

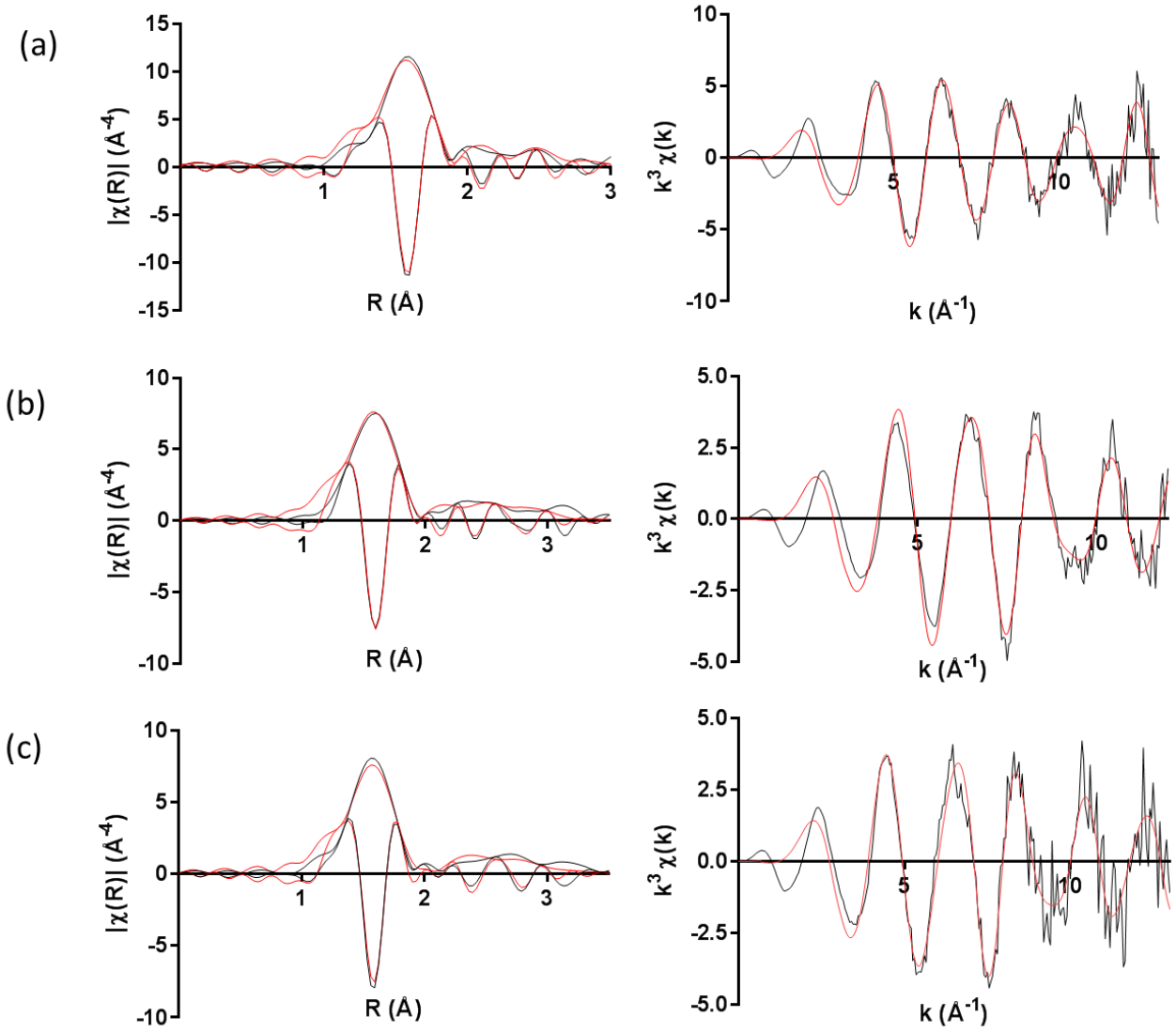

Fig. S12. (left) Rh K-edge k^3-weighted EXAFS signal, and (right) corresponding Fourier transforms, fitted using parameters in **Table 2** for (a) fresh $RhNi/Al_2O_3$ (GR), (b) post-reaction $RhNi/Al_2O_3$ (GR), and (c) Rh/Al_2O_3. Black lines represent experimental data and red lines are fits.

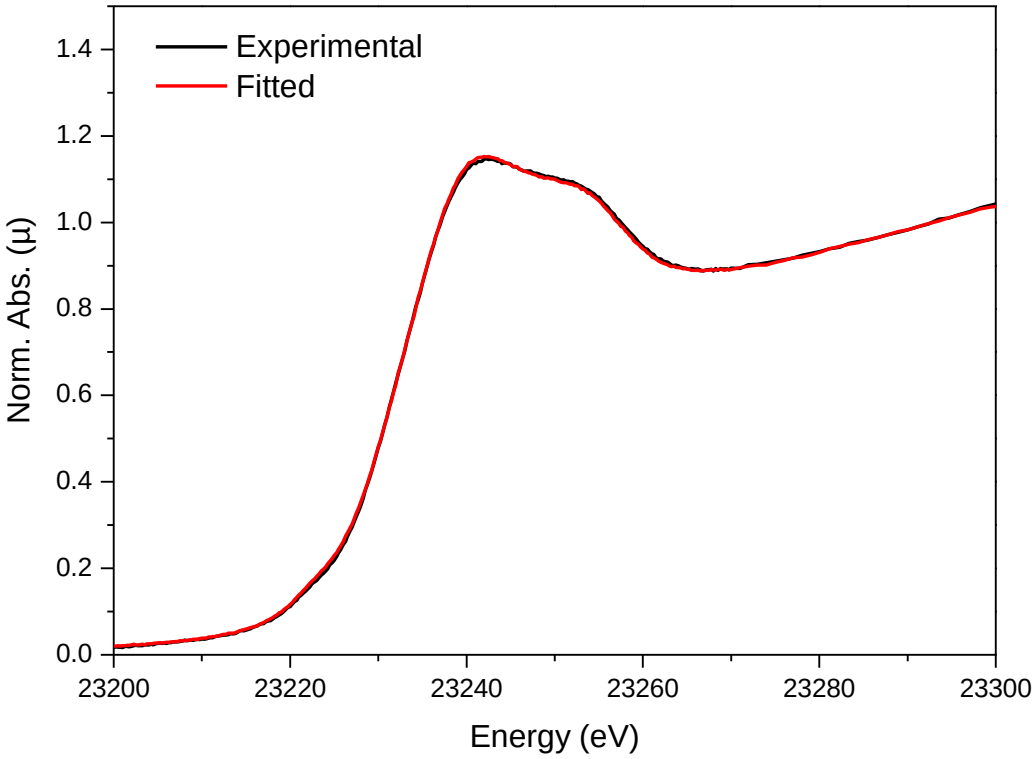

Fig. S13. Linear combination fit of edge-step normalised XANES of $RhNi/Al_2O_3$ (CR). Fitted XANES spectrum is a superposition of 25 % $RhNi/Al_2O_3$ (GR) and 75 % Rh/Al_2O_3.

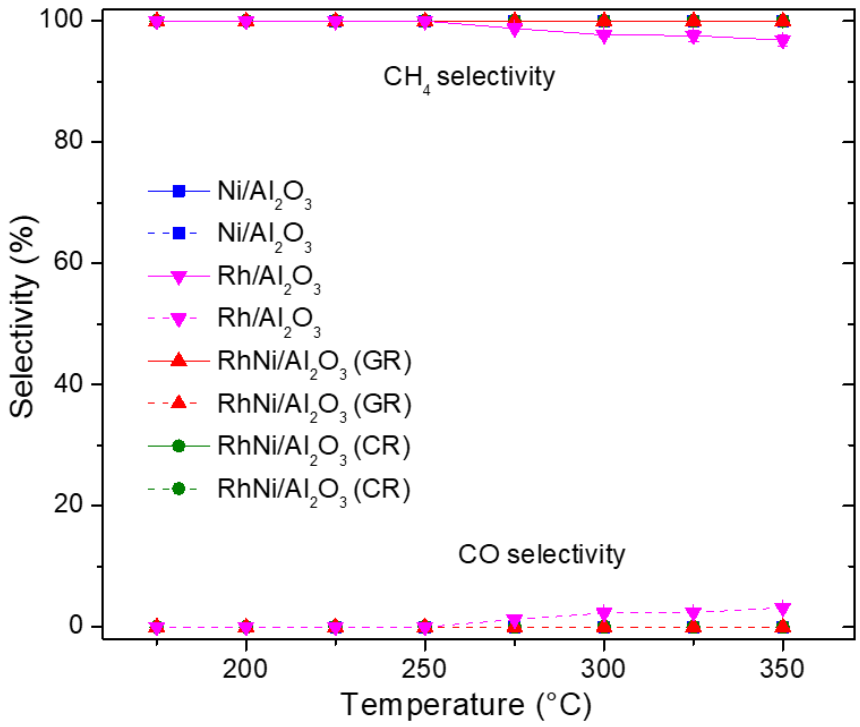

Fig. S14. CH_4 and CO selectivity during CO_2 methanation over Ni/Al_2O_3, Rh/Al_2O_3, $RhNi/Al_2O_3$ (GR), and $RhNi/Al_2O_3$ (CR).

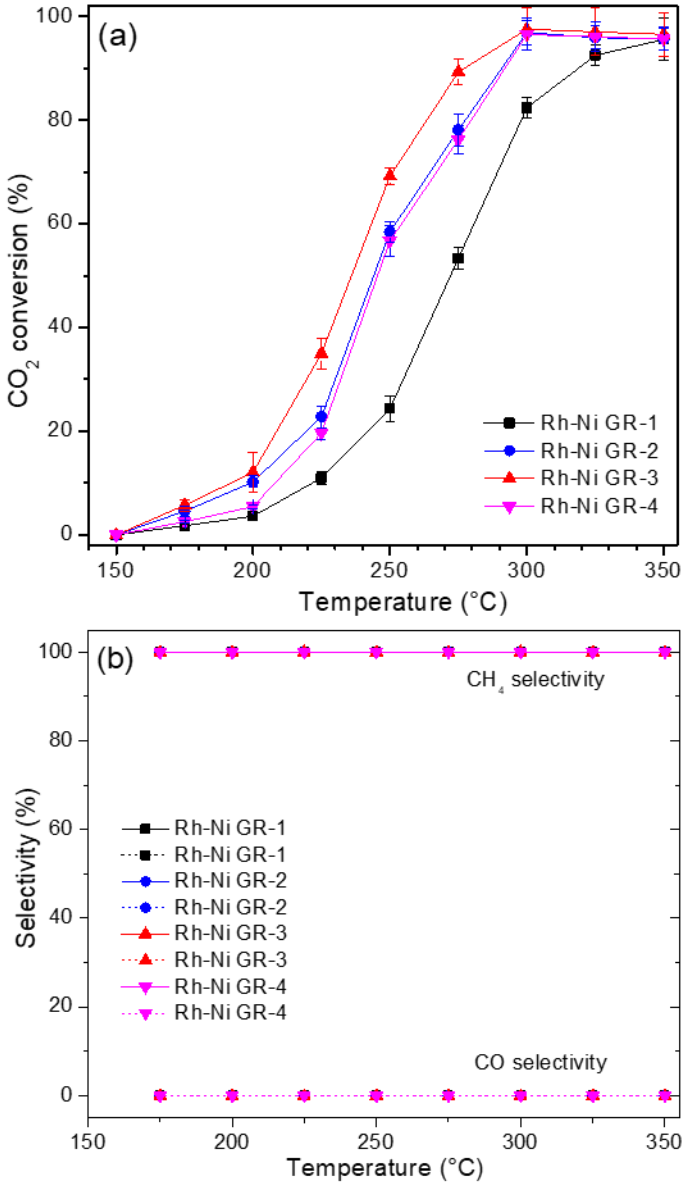

Fig. S15. Effect of Rh precursor concentration on (a) CO_2 conversion versus reaction temperature, and (b) CH_4 and CO selectivity during CO_2 methanation over $RhNi/Al_2O_3$ catalysts prepared by galvanic replacement.

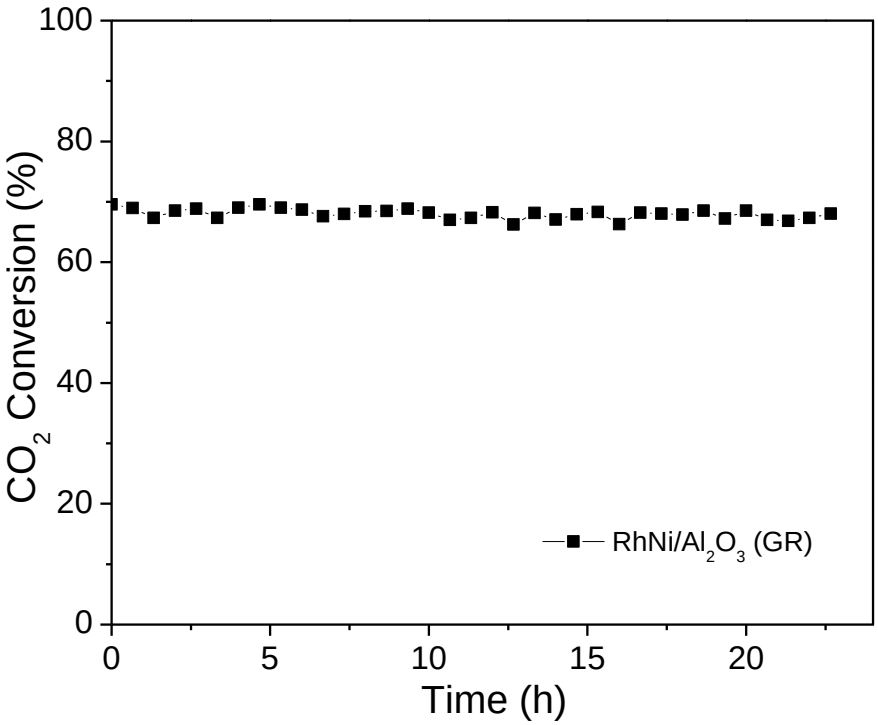

Fig. S16. CO_2 conversion versus time on-stream during methanation over RhNi/Al_2O_3 (GR). Reaction conditions: 250 °C; reactant gas mix = 5% CO_2, 20% H_2, 75% N_2; total flow rate = 40 mL/min; GHSV = ca. 48,000 mL/(g h).

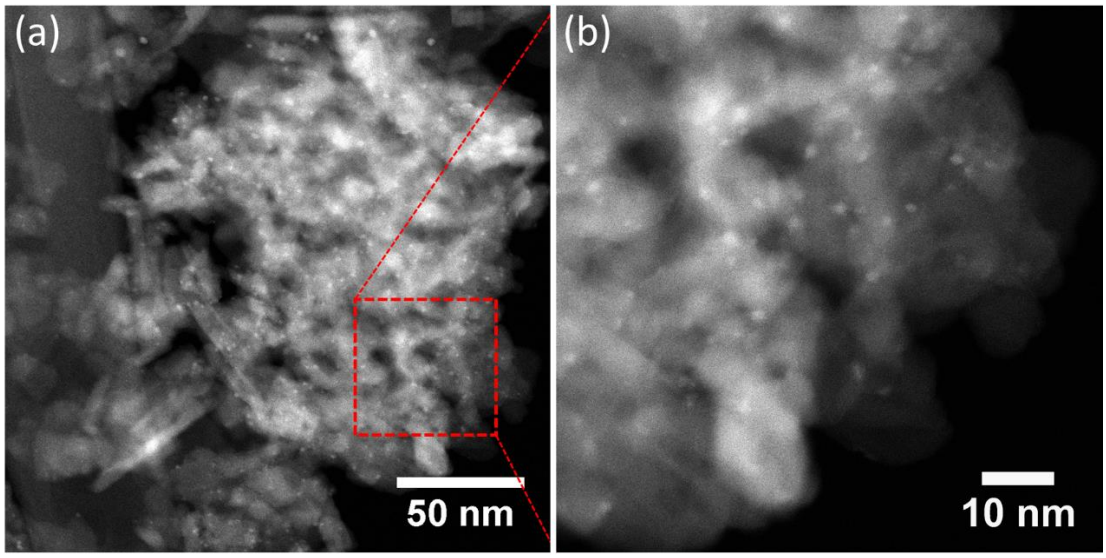

Fig. S17. (a, b) HAADF-STEM images of post-reaction RhNi/Al_2O_3 (GR) from the stability test in **Fig. S16**.

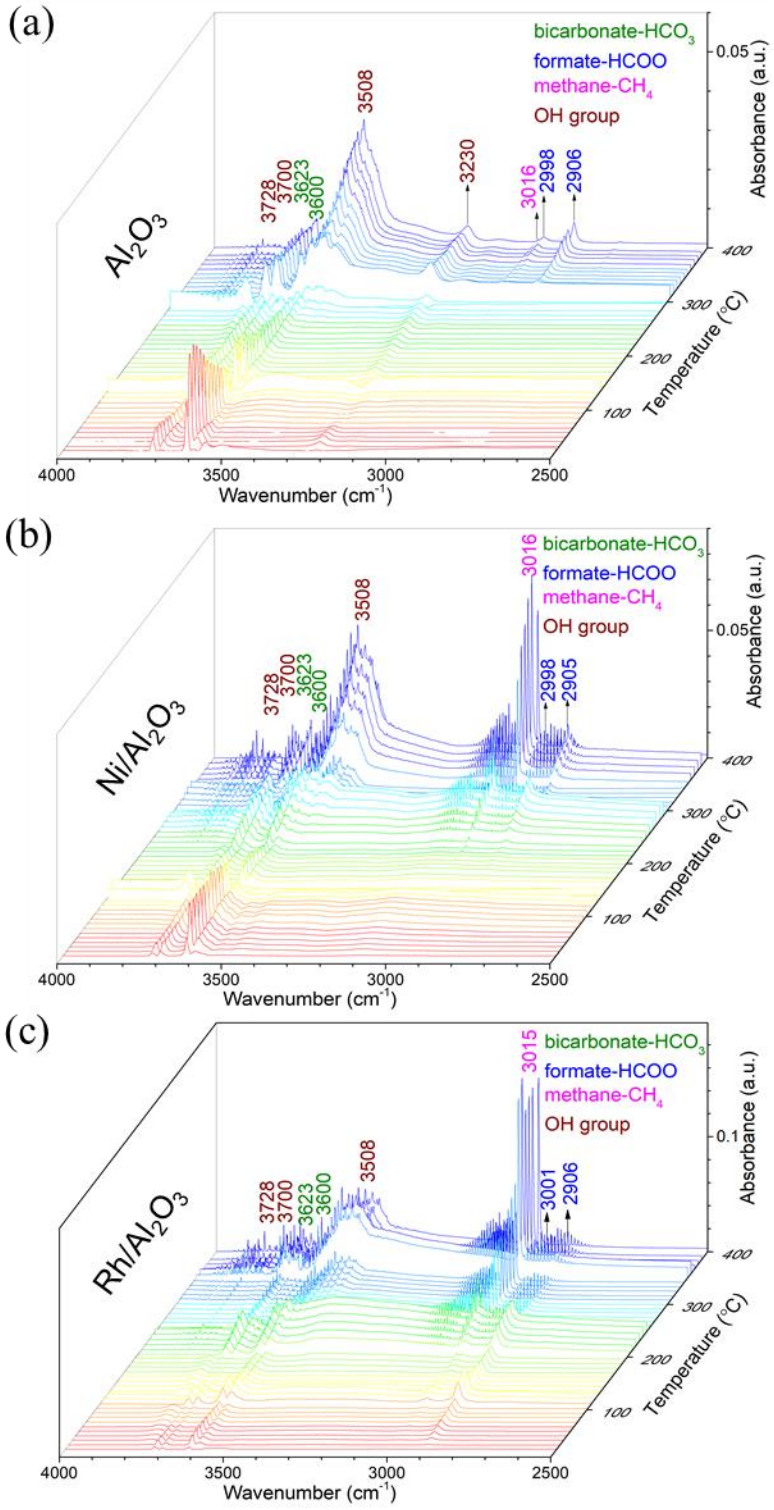

Fig. S18. In-situ DRIFTS spectra in the wavenumber rage from 4000 to 2500 $cm^{-1}$of (a) Al_2O_3, (b) Ni/Al_2O_3, (c) Rh/Al_2O_3 for CO_2 methanation from 30-400 °C (CO_2:H_2:Ar=2:8:30, 40 mL/min total).

ICP-MS results in **Table S1** quantify the elemental compositions of catalysts. With increasing Rh^{3+} precursor concentration during the GR process, the Rh loading increased from 0.22 wt% (for RhNi GR-1) to 1.08 wt% (for RhNi GR-3); further increases in the Rh^{3+} precursor concentration did not increase the Rh loading (RhNi GR-4, 1.01 wt%) indicating that the maximum loading attainable by GR was 1 wt% Rh. The decrease in Ni concentration for RhNi GR-1, 2, and 3 is a consequence of the galvanic replacement process in which Rh^{3+} ions exchange for metallic Ni atoms. The similar Ni concentrations of RhNi GR-3 and 4 reflects their similar Rh loadings. Since RhNi GR-3 possessed the highest Rh loading it was selected for detailed investigation in this work. For simplicity, RhNi GR-3 is referred to as $RhNi/Al_2O_3$ (GR) within the main text.

Table S1. Preparation method, weight percentage of Ni and Rh, specific surface area, Rh:Ni molar ratio for Ni/Al_2O_3, Rh/Al_2O_3, $RhNi/Al_2O_3$ (CR), and $RhNi/Al_2O_3$ (GR) samples.

Catalyst	Preparation method[a]	Weight percentage from ICP-MS		Specific surface area	Rh:Ni molar ratio
		Ni (wt%)	Rh (wt%)	(m^2 g^{-1})	
Ni/Al_2O_3	CR	1.89	-	177	-
Rh/Al_2O_3	CR	-	1.18	174	-
$RhNi/Al_2O_3$ (CR)	CR	1.79	0.91	197	0.29
RhNi GR-1	GR	1.90	0.22	167	0.07
RhNi GR-2	GR	1.88	0.69	165	0.21
RhNi GR-3 ≡ ($RhNi/Al_2O_3$ (GR))	GR	1.56	1.08	160	0.39
RhNi GR-4	GR	1.60	1.01	162	0.36

[a]CR = chemical reduction; GR = galvanic replacement.

Table S2. Comparative catalytic activity of Rh catalysts for CO_2 methanation.

Catalyst	Preparation method	Reaction temperature (°C)	TOF[a] (s^{-1})	Ref.
$RhNi/Al_2O_3$ (GR)	galvanic replacement	250	2.8×10^{-3}	Current study
$RhNi/Al_2O_3$ (CR)	chemical reduction	250	6.5×10^{-3}	Current study
$Rh\text{-}Al_2O_3$	impregnation	267	1.6×10^{-3}	[3]
$Rh\text{-}SrTi_{0.7}Fe_{0.3}O_{3-\delta}$	impregnation	267	1.0×10^{-3}	[3]
$Rh\text{-}La_{0.6}Sr_{0.4}FeO_{3-\delta}$	impregnation	267	1.1×10^{-4}	[3]
Mesoporous Rh	template-assisted wet chemical reduction	450	5.0×10^{-3} (inert <350 °C)	[4]
Non-porous Rh	wet chemical reduction	450	1.3×10^{-3} (inert <350 °C)	[4]
Rh–Ni/3DOM LAO	in-situ H_2 reduction	250	6.7×10^{-4}	[5]
Rh/3DOM LAO	chemical reduction	250	2.8×10^{-4}	[5]

[a]Specific activity (based on CO_2 conversion) normalised per surface Rh atom.

References

[1] J. He, I. Ichinose, T. Kunitake, A. Nakao, Y. Shiraishi, N. Toshima, Facile fabrication of Ag−Pd bimetallic nanoparticles in ultrathin TiO_2-gel films: nanoparticle morphology and catalytic activity, J. Am. Chem. Soc., 125 (2003) 11034-11040.

[2] X. Yu, J. He, D. Wang, Y. Hu, H. Tian, Z. He, Facile controlled synthesis of Pt/MnO_2 nanostructured catalysts and their catalytic performance for oxidative decomposition of formaldehyde, J. Phys. Chem. C, 116 (2012) 851-860.

[3] R. Thalinger, T. Götsch, C. Zhuo, W. Hetaba, W. Wallisch, M. Stöger-Pollach, D. Schmidmair, B. Klötzer, S. Penner, Rhodium-catalyzed methanation and methane steam reforming reactions on rhodium–perovskite systems: metal–support interaction, ChemCatChem, 8 (2016) 2057-2067.

[4] H. Arandiyan, K. Kani, Y. Wang, B. Jiang, J. Kim, M. Yoshino, M. Rezaei, A.E. Rowan, H. Dai, Y. Yamauchi, Highly selective reduction of carbon dioxide to methane on novel mesoporous Rh catalysts, ACS Appl. Mater. Interfaces, 10 (2018) 24963-24968.

[5] H. Arandiyan, Y. Wang, J. Scott, S. Mesgari, H. Dai, R. Amal, In situ exsolution of bimetallic Rh-Ni nano-alloys: highly efficient catalyst for CO_2 methanation, ACS Appl. Mater. Interfaces, 10 (2018) 16352-16357.